IEEE Access
Multidisciplinary | Rapid Review | Open Access Journal

IEEE POWER & ENERGY SOCIETY SECTION

Received 19 February 2024, accepted 21 March 2024, date of publication 25 March 2024, date of current version 5 April 2024.

Digital Object Identifier 10.1109/ACCESS.2024.3381781

RESEARCH ARTICLE

Fine-Grained Modeling and Coordinated Scheduling of Source-Load With Energy-Intensive Electro-Fused Magnesium Loads

YIBO WANG[1], (Member, IEEE), ZIKANG YANG[1], XUDONG ZHAO[1], HONGDAN LIU[1], DONGZHE WANG[1], AND CHUANG LIU[2], (Member, IEEE)

[1]Key Laboratory of Modern Power System Simulation and Control and Renewable Energy Technology, Northeast Electric Power University, Jilin 132012, China
[2]School of Electrical Engineering, Northeast Electric Power University, Jilin 132012, China

Corresponding author: Yibo Wang (wangyibofangyuan@126.com)

ABSTRACT With the rising adoption of renewable energy sources worldwide, the uncertainty within electrical power systems is amplifying, leading to rising challenges in wind power assimilation and operational costs. In addressing these pressing issues, this research emphasizes a sophisticated modeling technique for the energy-intensive electro-fused magnesium loads on demand. Furthermore, we introduce a coordinated scheduling approach for power systems, harnessing the regulatory capabilities of these loads. Initially, an in-depth analysis of the characteristics of the electro-fused magnesium energy-intensive load is carried out, from which a refined model is developed. Subsequently, considering the flexible regulatory potential of the electro-fused magnesium furnace apparatus, a bi-level optimization scheduling model is crafted, prioritizing the maximization of wind power absorption at the upper level and minimizing system operational costs at the lower level. The efficacy and rationale of the proposed methodology are corroborated through computational analyses.

INDEX TERMS Refined modeling, wind power integration, operational costs, optimal scheduling.

I. INTRODUCTION

Wind energy has emerged as a fundamental pillar in achieving net-zero emissions by 2050. In 2022, wind energy generation saw a significant increase of 265 TWh, marking a 14% growth and exceeding the 2 TWh threshold [1]. However, wind energy's inherent characteristics, such as variability, intermittency, and non-dispatchable nature, intensify peak-to-valley disparities in the load curve with extensive grid integration [2]. During low demand periods, thermal power stations must reduce their output, sometimes beyond their minimum generation capacities, posing risks of system disruptions [3], [4], [5]. Following the proliferation of smart grids, interest in demand response mechanisms has increased. Utilizing adjustable demand-side resources for achieving harmonized source-load alignment offers a viable solution to enhance wind energy absorption, reduce peak-load stress, and address grid management challenges [6]. Recent research, both domestic and international, highlights the role of demand-side loads in grid management, contributing to the absorption of curtailed wind energy and alleviating power system peak loads. Additionally, reference [9] supports the use of price-incentive-driven demand-side assets, offering flexible load profiles that shift wind energy production from off-peak to peak periods, encouraging broader wind power integration.

While the studies above have made noteworthy contributions, they primarily focus on loads with limited capacities, resulting in less discernible effects in accommodating wind energy. In contrast, energy-intensive loads such as electric arc furnaces and electrically-fused magnesium industrial devices usually boast significant capacities,

The associate editor coordinating the review of this manuscript and approving it for publication was Cuo Zhang.

offering a more pronounced adjustment scope during demand response Schemes [10]. Such energy-intensive loads inherently demand vast electricity volumes. Utilizing clean and economical wind energy for their daily operations can significantly curtail production costs [11], [12]. Additionally, these loads typically represent pre-existing local demands. When juxtaposed against emerging loads, energy-intensive loads possess more mature demand response techniques, lower risks, and utilization costs, making them ideal candidates for local wind energy absorption without imposing substantial infrastructural costs [13], [14]. Recent works have investigated the participation of energy-intensive loads in power system scheduling and renewable energy integrated management, utilizing these loads to scrutinize economic benefits and operational expenses. One notable study simulated the dynamic regulation abilities of such loads based on intricate production processes, introducing a bi-level optimization model for wind and photovoltaic generation capacity allocation to augment renewable penetration in hybrid systems [15]. Another presented a two-stage complementary peak-shaving strategy for energy-intensive loads utilizing battery storage systems, instituting an optimization model to minimize system operations and curtail costs [16]. Moreover, a robust, Scheme-adjustable scheduling model was formulated, achieving reductions in energy costs and enhancing wind power utilization [17].

The Haicheng region in Liaoning Province is replete with mineral resources, with proven magnesite reserves amounting to 2640 million tons, constituting 61.8% of China's total and a quarter of global funds, making it a pivotal magnesite industrial base with abundant energy-intensive electrically-fused magnesium loads [18]. This region also has rich wind resources, necessitating high-capacity loads with thermal power for local absorption. Currently, controllable load regulation platforms have been integrated into local magnesite processing companies, capturing real-time operational feedback from the electrically-fused magnesium furnaces, allowing comprehensive monitoring of their load statuses and enabling quick and flexible load adjustments, offering novel flexibility to the grid [19].

Recent studies have concentrated on controlling currents in electrically-fused magnesium furnaces. A novel adaptive PID controller was developed to regulate the melting current within desired ranges, achieving substantial energy conservation [20]. A data-driven anomaly detection and self-healing control system was introduced, where corrective current adjustments are made based on detection outcomes to mitigate irregular furnace operations [21]. Employing state-of-the-art nonlinear control tools, another study ensured that the three-phase currents converge within setpoint vicinities, addressing the engineering challenge of stable current control in such furnaces [22]. These contributions offer solutions for sound current management in electrically-fused magnesium furnace electrodes. In practical production and dispatch processes, setting three-phase current values in the furnaces can regulate their load magnitude, aiding in wind energy absorption in conjunction with thermal power units [23]. However, these references overlook detailed modeling concerning specific production processes, demand response patterns, and control capabilities of these loads, failing to capture their genuine impacts on the grid.

Current research on the participation of energy-intensive electro-fused magnesium loads in dispatch models is not comprehensive, as it has only considered specific types of energy-intensive electro-fused magnesium loads and lacks optimization modeling that incorporates the specific production characteristics of these loads. The main contribution of this paper is that based on the analysis of the characteristics of energy-intensive electro-fused magnesium loads, we have developed a refined model for these loads. Then, by utilizing the adjustable capacity of energy-intensive electro-fused magnesium loads to mitigate wind power forecasting errors and coordinating with traditional thermal power units, we have established a bi-level optimization dispatch model for electric smelting magnesium furnaces. This model aims to maximize wind power consumption and minimize the system's operational costs through source-load coordination. Finally, we conducted a case study analysis using a multi-objective genetic algorithm from heuristic algorithms, validating the model's effectiveness and rationality.

II. CHARACTERIZATION AND REFINED MODELING OF ELECTRO-FUSED MAGNESIUM ENERGY-INTENSIVE LOAD

A. CHARACTERIZATION OF ELECTRO-FUSED MAGNESIUM ENERGY-INTENSIVE LOAD

The electro-fusion of magnesium ore in furnaces, as illustrated in Figure 1, constitutes a crucial method widely employed in the magnesium industry. This metallurgical process is heavily dependent on a significant input of electrical energy, which positions the electro-fused magnesium industry as a notably energy-intensive sector and classifies the furnace as a significant energy-intensive load.

During the operation of the electro-fused magnesium furnace, consistent voltage and substantial current are imperative to ensure the internal temperature remains within a specified range. Between these temperature extremes, the ''feasible temperature domain'' exists, within which the electro-fused magnesium furnace operates safely and produces magnesium products of the desired quality.

Given that the thermal energy within the furnace is derived from electric power, this ''temperature feasibility region'' equates to a ''power feasibility region'' for the furnace, indicating the adjustable power range available during the furnace's operation. Within this domain, power modulation of the furnace is achievable through its internal signal detection mechanisms. In summary, the electro-fused magnesium furnace exhibits adjustable and controllable power characteristics during its production operations.

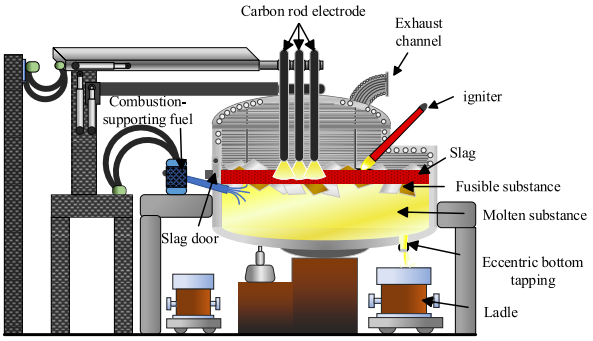

FIGURE 1. Schematic diagram of the working principle of the electro-fused magnesium furnace.

B. REFINED MODELING OF ELECTRO-FUSED MAGNESIUM ENERGY-INTENSIVE LOAD

The task of developing refined models for the energy-intensive load of electro-fused magnesium is complex and requires specialized expertise. It usually requires an interdisciplinary approach, incorporating expertise in electrical engineering, materials science, chemical engineering, and thermodynamics. This study primarily concentrates on the electrical port modeling of the electro-fused magnesium energy-intensive load, Analyzing the production process of the electro-fused magnesium furnace reveals three distinct phases: preheating, melting, and extinguishing, as depicted in Figure 2.

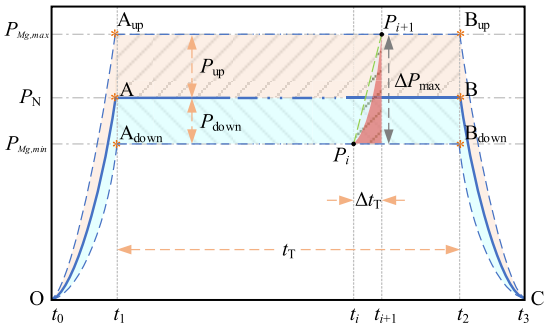

FIGURE 2. Schematic power curve diagram for the electric melting magnesium furnace production process.

Preheating Phase (interval t_0-t_1): The primary objective of this Phase is to elevate the temperature of the furnace body and the raw materials within, preparing them for subsequent melting and reactions.

The ideal curve for this procedure is represented as segment OA in Figure 2. During the t_0-t_1 interval, the power displays an ascending trend, rising from 0 to P_N.

Melting Phase (interval t_1-t_2): The goal is to melt the preheated materials using electric arcs or other heating methods, followed by chemical reactions to produce magnesium metal.

Segment AB represents the ideal trajectory during this Phase in Figure 2. During the t_1-t_2 interval, the power manifests a steady-state behavior, consistently maintained at P_N

Shutdown Phase (interval t_2-t_3): This Phase aims to safely terminate the operations of the electro-fused magnesium furnace after all reactions have concluded.

The ideal progression for this Phase is illustrated as segment BC in Figure 2. Throughout the t_2-t_3 interval, the power exhibits a declining trend, transitioning from P_N to 0.

The three intervals above depict the power modulation phases during the electro-fused magnesium furnace's operation. The blue trajectory OABC in Figure 2 signifies the optimal power operational curve for the furnace across these phases in an ideal Scheme. The models for current and power under this curve are represented in Equation (1) and Equation (2), respectively.

$$I(t) = \begin{cases} \lambda t & (t \le t_1) \\ I_n & (t_1 < t < t_2) \\ I_n - (t - t_2) & (t > t_2) \end{cases} \tag{1}$$

$$P(t) = \sqrt{3} U I(t) \cos\varphi = \begin{cases} \delta t & (t \le t_1) \\ P_n & (t_1 < t \le t_2) \\ P_n - \delta(t - t_2) & (t > t_2) \end{cases} \tag{2}$$

$$\delta = \sqrt{3}\lambda U \cos\varphi \tag{3}$$

The equations are defined with the following parameters: $I(t)$ is the melting current value of the electro-fused magnesium furnace at time t; λ is the recent increase coefficient; I_n denotes the set current for phase n within the working cycle; $P(t)$ represents the active power at time t; U is the melting voltage value; $\cos\varphi$ is the power factor of the power supply system; δ is the power amplification coefficient; and P_n is the preset or rated power of the furnace.

The power of practical electro-fused magnesium furnaces doesn't strictly follow the ideal blue curve OABC. This deviation is due to current, voltage, raw material properties, furnace structure, operational parameters, environmental conditions, chemical reaction states, and the control system, necessitating careful consideration and optimization.

Considering the electro-fused magnesium furnace's production processes and technological peculiarities, a specific "temperature feasibility region" is apparent during the preheating, melting, and shutdown phases. Correspondingly, there's a "power feasibility region" for each Phase, depicted by the shaded area in Figure 2, which implies varying control intervals for the furnace's power across its operational stages, with the upper and lower constraints represented by the dashed lines $OA_{up}B_{up}C$ and $OA_{down}B_{down}C$ in Figure 2. The rules for capacity adjustments are as follows:

$$P^t = P_{pre} + S_1^t N_{Mg}^t P_{up} - S_2^t N_{Mg}^t P_{down} \tag{4}$$

$$S_1^t + S_2^t \le 1 \tag{5}$$

$$P_{int-ve,max} \le P(t) \le P_{int-ve,min} \tag{6}$$

$$P_{int-ve,max} = \begin{cases} a_1 t^2 + b_1 t + c_1 & (t \le t_1) \\ P_n & (t_1 < t \le t_2) \\ a_2 t^2 + b_2 t + c_2 & (t > t_2) \end{cases} \tag{7}$$

$$P_{\text{int}-ve,\min} = \begin{cases} a_3 t^2 + b_3 t + c_3 & (t \le t_1) \\ P_n & (t_1 < t \le t_2) \\ a_4 t^2 + b_4 t + c_4 & (t > t_2) \end{cases} \tag{8}$$

In the given context, P_{pre} delineates the standard operating power of the electro-fused magnesium furnace at time t. Meanwhile, $N_{\text{Mg}}(t)$ simultaneously quantifies the number of furnaces available for power modulation. The terms P_{up} and P_{down} denote the power adjustment margins (increase and decrease) for an individual furnace. The state variables S_1^t and S_2^t, set to 1, signify power ramp-up and ramp-down of the stove at t, respectively. Further, $P_{\text{int}-ve,\max}$, and $P_{\text{int}-ve,\min}$ are constraints representing the maximal and minimal power limits for safe furnace operation. The coefficients a_i, b_i, and c_i (where $i \in \{1,2,3,4\}$) characterize the power boundaries during the preheating and shutdown phases.

It's pivotal to understand that power modulation in the furnace, across varying active stages, is dictated by multiple factors—equipment degradation risks, purity of the magnesium product, energy conversion efficiency, and production safety.

Consequently, swift power transitions, termed "ramping constraints," are proscribed, Such ramping constraints, integral to the manufacturing and power provisioning schema, are thoroughly discussed in the succeeding sections.

$$RD_g \le \left| P_{m,t_i} - P_{m,t_{i-1}} \right| \le RU_g \tag{9}$$

Within the presented framework, $P_{m,ti}$, and $P_{m,ti-1}$ designate the power values at moments t_i and t_{i-1}, respectively. Symbols RD_g and RU_g elucidate the maximum power variations—both increases and decreases—that the electro-fused magnesium furnace can undergo within a unit timeframe, encapsulating the essence of ramping constraints.

However, electric smelting magnesium furnaces have certain power adjustment flexibility during different production stages (preheating, melting, and shutdown), but adjustments cannot be made arbitrarily or frequently, meaning the equipment is subject to adjustable state constraints:

$$P_{\text{F}} = P_{\text{pre}} + \mu_{\text{F}} P_{\text{adj-st}} \tag{10}$$

In the given context, μ_{F} is the state variable, which assumes values of either 0 or 1, while $P_{\text{adj}-\text{st}}$ denotes the adjustable quantity.

Moreover, the electric energy requisite for producing a furnace's worth of magnesium product remains relatively consistent, leading to the following energy balance constraint:

$$\sum_{t=1}^{T_{\text{Mg}}} P_{\text{H},k}^t = 0 \tag{11}$$

Within the specified framework, T_{Mg} denotes the operational cycle of the electro-fused magnesium furnace, whereas $P_{\text{H},k}^t$ corresponds to the power values throughout its various active stages.

III. SOURCE-LOAD COORDINATED OPTIMIZATION SCHEDULING WITH REFINED ENERGY-INTENSIVE ELECTRO-FUSED MAGNESIUM LOAD MODEL

In response to the burgeoning need for sustainable energy solutions, our study introduces an innovative source-load coordinated optimization scheduling approach, leveraging the refined model of energy-intensive electro-fused magnesium loads. Central to our methodology is a bi-level optimization framework. The upper tier of this framework is dedicated to maximizing the absorption of wind power, seamlessly integrating fluctuating renewable energy sources into the power mix without compromising on stability or efficiency. Concurrently, the lower tier focuses on minimizing operational costs, ensuring that the power system operates economically while accommodating the variable nature of renewable energy.

The idea of the model is as follows: The coordinated scheduling method involving energy-intensive electro-fused magnesium loads is designed to harness the adjustable, rapidly responsive, and high-capacity characteristics of these loads. This approach aims to mitigate the fluctuations of wind power generation under the premise of adhering to the intrinsic regulatory properties of electro-fused magnesium loads, thereby enhancing the operational stability of the system post-renewable energy integration. During periods of high wind power output, the consumption by energy-intensive electro-fused magnesium loads is increased, whereas it is decreased during periods of low wind power output. This strategy absorbs the excess wind power that traditional thermal power units struggle to manage during peak production times, thus enhancing the utilization rate of renewable energy sources. By smoothing out the variability in wind power after grid integration, the method concurrently reduces the frequency of deep adjustments required by thermal power units, lowering their operational costs and enhancing overall energy utilization efficiency.

A. UPPER-LAYER OPTIMIZATION MODEL TARGETING MAXIMUM WIND POWER INTEGRATION

To encapsulate the global emphasis on wind power development, alongside the pressing imperatives of carbon emission reduction and enhancing energy sustainability, the upper layer of the bi-level optimization framework prioritizes the maximization of wind power integration.

$$\max P_{\text{W-act}} = \sum_{t=1}^{T} \sum_{i=1}^{N_{\text{wind}}} P_{\text{W-act},i}^t \Delta T \tag{12}$$

In the described model, T represents the total number of time intervals within the dispatching cycle. N_{wind} signifies the count of wind farms. $P_{\text{W}-\text{act},i}^t$ indicates the power output of wind farm i during the time interval t.

The constraints predominantly encompass operational limitations of the power system, output restrictions for both wind and thermal power units, and power control constraints for the energy-intensive electric magnesium smelting load.

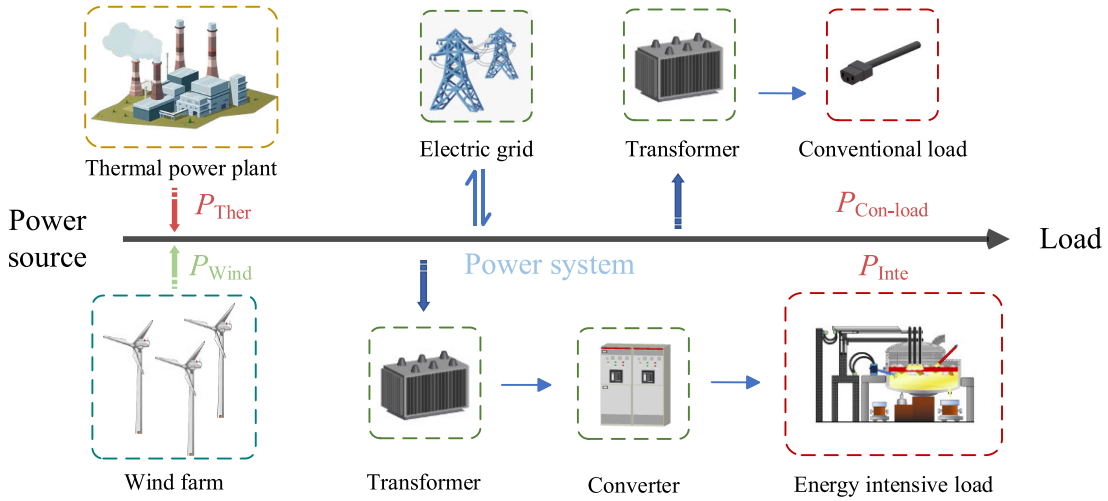

FIGURE 3. Schematic of power system with source-load coordination incorporating energy-intensive loads.

1) System Operational Constraints:

- Power Balance Constraint:

$$\sum_{i=1}^{T} P^t_{\text{W-act},i} + P^t_{\text{Ther}} = P^t_{\text{Load-fore}} + \sum_{k=1}^{N_{\text{Mg}}} (P^t_{\text{Mg},k} + P^t_{\text{H},k}) \tag{13}$$

In the given formulation, P^t_{Ther} denotes the total active power output of the thermal power unit during time interval t. $P^t_{\text{Load-fore}}$ represents the forecasted active power of the system's conventional load at time t. N_{Mg} specifies the number of electric magnesium smelting furnaces. For each furnace, $P^t_{\text{Mg},k}$ is the active power during the time interval t, and $P^t_{\text{H},k}$ portrays its regulation power in the same period.

- Spinning Reserve Constraint:

$$P^{\max}_{Ther} - P^t_{Ther} \geq R^t_{\text{L},+} + R^t_{W,+} \tag{14}$$

$$P^t_{Ther} - P^{\min}_{Ther} \geq R^t_{\text{L},-} + R^t_{W,-} \tag{15}$$

$R^t_{\text{L},+}$ and $R^t_{\text{L},-}$ denote the positive and negative spinning reserves required during time intervals to address load forecasting errors. Similarly, $R^t_{\text{W},+,}$ and $R^t_{\text{W},-}$ represent the positive and negative spinning reserves needed at times to counteract wind power forecasting discrepancies.

2) Wind Power Output Constraints:

$$0 \leq P^t_{\text{W},i} \leq P^t_{\text{W-pre},i} \tag{16}$$

The given formulation, $P^t_{W-pre,i}$ represents the active power forecasted output for wind farm i during time interval t.

3) Thermal Power Unit Operational Constraints:

- Boundaries for Output Power:

$$P_{\text{Ther min}} \leq P^t_{\text{Ther}} \leq P_{\text{Ther max}} \tag{17}$$

- Ramp Rate Constraints for Thermal Power Units:

$$P^t_{\text{Ther}} - P^{t-1}_{\text{Ther}} \leq P_{\text{Ther up}} \tag{18}$$

$$P^{t-1}_{\text{Ther}} - P^t_{\text{Ther}} \leq P_{\text{Ther down}} \tag{19}$$

The preceding model integrates constraints considering the operating dynamics of conventional thermal power units, mainly focusing on their ramping abilities. Specifically, P^{t-1}_{Ther} represents the net active power output of the traditional unit during the interval $t-1$. The parameters $P_{\text{Ther up}}$ and $P_{\text{Ther down}}$ denote the thermal units' positive and negative ramp rates, respectively.

4) Constraints for Regulating Power of Energy-intensive Electromagnetic Magnesium Load:

- Bounds on Regulating Power:

$$P_{\text{H min}} \leq \sum_{k=1}^{N_{\text{Mg}}} P^t_{\text{H},k} \leq P_{\text{H max}} \tag{20}$$

Herein, P_{Hmax} and P_{Hmin} stipulate the upper and lower limits for the regulating power of the electromagnetic magnesium load.

- Constraint on Regulation Frequency:

$$0 \leq \sum_{t=1}^{T} \left| S^t_{\text{H}} - S^{t-1}_{\text{H}} \right| \leq M \tag{21}$$

In this context, S^t_{H} and S^{t-1}_{H} symbolize the regulation state variables for the electromagnetic magnesium energy-intensive load during intervals t and $t-1$, respectively. A state of $S^t_{\text{H}} = 1$ indicates active regulation at the moment t, whereas $S^t_{\text{H}} = 0$ signifies no such engagement.

- Ramping Constraints for Electromagnetic Magnesium Load:

$$P^t_{\text{H}} - P^{t-1}_{\text{H}} \leq P_{\text{H, up}} \tag{22}$$

$$P^{t-1}_{\text{H}} - P^t_{\text{H}} \leq P_{\text{H, down}} \tag{23}$$

Here, P_{H}^{t} and P_{H}^{t-1} denote the active power output of the conventional unit at intervals t and $t-1$, respectively. Meanwhile, $P_{\mathrm{H.,up}}$ and $P_{\mathrm{H,down}}$ capture the positive and negative ramp rates.

- Energy Balance Constraint for Regulation:

$$\sum_{t=1}^{T_{\mathrm{Mg}}} P_{\mathrm{H},k}^{t} = 0 \tag{24}$$

T_{Mg} indicates the number of intervals for one electromagnetic magnesium furnace operating cycle.

B. LOWER-LEVEL OPTIMIZATION MODEL TARGETING MINIMAL SYSTEM OPERATIONAL COSTS

Building on the groundwork laid by the upper-level optimization model, we develop a lower-tier optimization framework with a primary objective to minimize system operational costs. This objective integrates the operating expenditures of thermal power units and factors in penalties arising from wind curtailment.

$$\min F = M_{\mathrm{G}} + M_{\mathrm{W}} \tag{25}$$

$$M_{\mathrm{G}} = \sum_{t=1}^{T}\sum_{j=1}^{N_{\mathrm{G}}} U_{\mathrm{G}j}^{t}\left[a_j\left(P_{\mathrm{G}j}^{t}\right)^2 + b_j P_{\mathrm{G}j}^{t} + c_j\right] \tag{26}$$

$$M_{\mathrm{W}} = \sum_{t=1}^{T}\sum_{i=1}^{N_{\mathrm{W}}} \eta\left(P_{\mathrm{Wind\text{-}fore},i}^{t} - P_{\mathrm{Wind},i}^{t}\right)\Delta T \tag{27}$$

where M_{G} symbolizes the operational costs of thermal power units; C_{abon} indicates penalties for wind curtailment in the system; U_{Gj}^{t} represents the active status of the thermal power unit j during time t (with U_{Gj}^{t} =0 signifying its offline status and U_{Gj}^{t} =1 indicating it's running); a_j, b_j, c_j are the cost parameters of thermal power unit j. The term η stands for the unit penalty cost for wind curtailment for wind farm i in the system, and ΔT embodies the total periods with wind curtailment.

The model's constraints encompass power balance for thermal power units, ramping restrictions, and bounds on output power, detailed as follows:

1) Power Balance Constraint for Thermal Units:

$$\sum_{t=1}^{T}\sum_{j=1}^{N_{\mathrm{G}}} P_{\mathrm{G}j}^{t} = \sum_{t=1}^{T} P_{\mathrm{G}}^{t} \tag{28}$$

where N_{G} defines the total number of thermal power units, and $P_{\mathrm{G}j}^{t}$ is the output of thermal power unit j during time t.

2) Ramping Speed Constraint for Thermal Units:

$$P_{\mathrm{G}j}^{t} - P_{\mathrm{G}j}^{t-1} \le P_{\mathrm{G}j,\mathrm{up}} \tag{29}$$

$$P_{\mathrm{G}j}^{t-1} - P_{\mathrm{G}j}^{t} \le P_{\mathrm{G}j,\mathrm{down}} \tag{30}$$

Here, $P_{\mathrm{G}j}^{t-1}$ is the output of thermal power unit j at time $t-1$, and $P_{\mathrm{G}j,\mathrm{up}}$ 和 $P_{\mathrm{G}j,\mathrm{down}}$ denote the ramp-up and ramp-down power limits, respectively, for unit j.

3) Output Power Boundaries for Thermal Units:

$$P_{\mathrm{G}j\,\min} \le P_{\mathrm{G}j}^{t} \le P_{\mathrm{G}j\,\max} \tag{31}$$

$P_{\mathrm{G}j\ \max}$ and $P_{\mathrm{G}j\ \min}$ represent the upper and lower output limits for thermal power unit j, respectively.

C. SOLUTION METHODOLOGY FOR THE MODEL

1) OBJECTIVE FUNCTION

$$\begin{cases} \begin{cases} \min G(x,y) \\ s.t. \quad h_i(x,y) = 0 \quad i = 1,2,\cdots,m \\ \qquad k_j(x,y) \le 0 \quad j = 1,2,\cdots,n \\ \quad x_{\min} \le x \le x_{\max}, \quad y \in \{0,1\} \end{cases} \\ \qquad\qquad \downarrow \\ \begin{cases} \min O(x,y) \\ s.t. \quad r_i(x,y) = 0 \quad i = 1,2,\cdots,u \\ \qquad s_j(x,y) \le 0 \quad j = 1,2,\cdots,v \\ \quad x_{\min} \le x \le x_{\max}, \quad t \in \{0,1\} \end{cases} \end{cases} \tag{32}$$

In addressing the intricacies of the bi-level optimization model developed in this study, which encompasses mixed-integer programming, we have strategically employed heuristic algorithms, with a particular emphasis on genetic algorithms (GAs), as our chosen solution approach. This decision is grounded in the recognition of the complex, multi-dimensional solution space that characterizes bi-level optimization problems, where traditional optimization techniques may fall short.

Heuristic algorithms, known for their flexibility and efficacy in navigating through vast and non-linear solution landscapes, offer a pragmatic pathway to identifying high-quality solutions. Within this broad category, genetic algorithms stand out due to their robust simulation of evolutionary processes, including selection, crossover, and mutation. These mechanisms enable GAs to effectively search for optimal solutions across a wide array of problem structures, making them particularly suitable for the dual-layered complexity inherent in our model.

The model developed in this study consists of two integral parts and falls under mixed-integer programming. A heuristic algorithm has been chosen as the solution approach to address this complex problem. The canonical form of the model and its resolution procedure are articulated as Equation(32). In Equation(32), G signifies the objective function of the upper level, while O represents that of the lower level. The variables, x, designated for optimization encompass outputs from thermal power units, planned wind power outputs, controllable power of energy-intensive electric magnesium furnaces, operational costs of thermal power units, and penalties associated with wind curtailment. Furthermore, the on-off statuses of both thermal and wind power units are pivotal decision variables. Throughout the solution process, the model is constrained by equality restrictions, including those for power balance in the system and thermal power units.

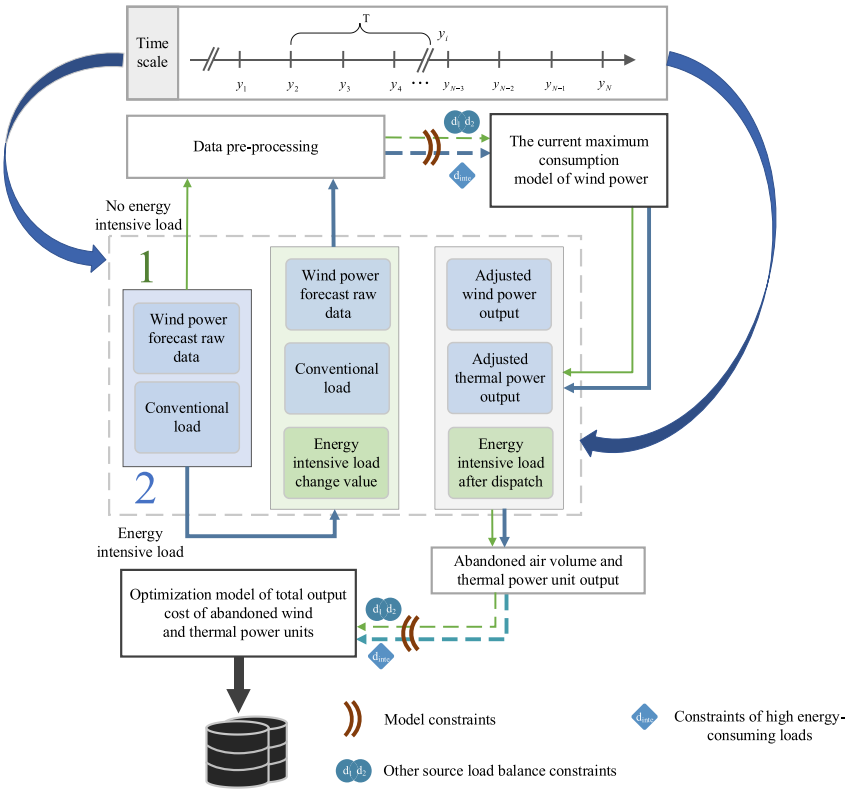

FIGURE 4. Flow chart of a dual-level optimal model of source-load coordination.

In addition, inequality constraints mainly consider the limitations on wind power output, operational rules for thermal power units, and regulations on the power adjustment for energy-intensive electric magnesium furnaces.

IV. CASE STUDY ANALYSIS

A. CASE DESCRIPTION

A simulation analysis is conducted under the following conditions to validate the efficacy and reasonableness of the proposed model: four thermal power units with a total capacity of 1500MW. The maximum P_{max} and minimum P_{min} outputs, along with operational cost parameters (*a, b, c*), are detailed in Table 1.

The wind power forecast and historical data in our study were constructed based on two key aspects: trend-wise, they adhere to the counter-peaking characteristic of wind energy; size-wise, they reflect the typical proportions of wind power output in the power system. This methodology ensures our data accurately simulates the operational dynamics between wind energy and system loads.

The wind farm boasts an installation capacity of 300MW and incurs a wind curtailment penalty rate of 350 yuan/(MW·h) per unit. The 24-hour conventional load and wind power output forecasts are depicted in Figure 5's clock chart. The total power of the energy-intensive electric magnesium furnace is set at 225MW, operating continuously for 24 hours, with up and down-regulation capabilities at 20%

TABLE 1. Operation parameters of thermal units.

Ther-para	P_{max}/（MW）	P_{min}/（MW）	*a*/ (m/MW²·h)	*b*/ (m/MW·h)	*c*/ (m/h)
G1	500	285	0.00048	16.19	1000
G2	400	230	0.00095	17.52	800
G3	300	188	0.00151	20.02	500
G4	300	188	0.00174	19.81	750

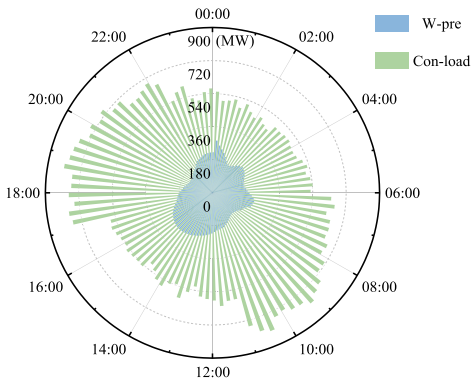

FIGURE 5. Predicted values of conventional load and wind power output.

and 15% of the rated power, respectively. Given the intricate reactions within the furnace during the preheating and

shutdown stages and the narrow ''power feasibility domain,'' its control range is not considered here.

In Figure 5, light green represents the conventional load forecast, and dark blue illustrates the wind power output forecast. As the figure suggests, the wind power output varies between 150-270MW, peaking between 22:00-01:00 and 12:00-14:00, whereas the conventional load oscillates between 500-800MW, peaking from 06:00-11:00 and 15:00-22:00. This case mirrors the counter-peaking characteristics of wind power, which intensifies the peak-adjusting pressure on thermal units and diminishes wind power utilization. We juxtapose a model excluding the electric magnesium energy-intensive load control (Scheme 1) against our refined co-optimization dispatching method that includes it (Scheme 2) under the same case conditions. Detailed comparative analysis ensues.

B. RESULTS ANALYSIS

Derived from the above case Schemes, Figures 6 and 7 present the outputs of thermal units and energy consumption of energy-intensive load electric magnesium furnaces under Schemes 1 and 2.

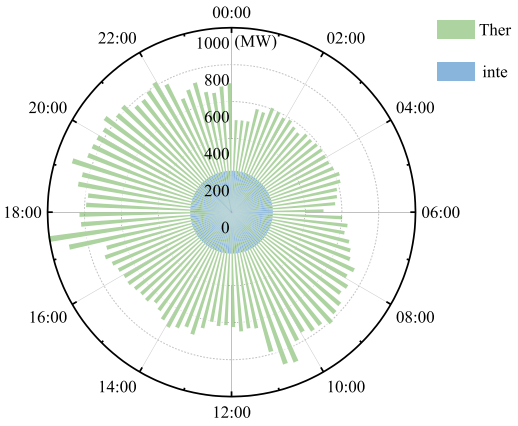

FIGURE 6. The output of thermal power units and the energy consumption of fused magnesium load (Scheme 1).

In Figure 6, 'Ther' and 'Inte' denote the four thermal units' cumulative outputs, energy consumptions, and the energy-intensive load furnace over 24 hours. Notably, in Scheme 1, the stove maintains consistent energy consumption, whereas the four thermal units exhibit minimal outputs during [00:00, 06:00], the day's trough, and escalate during [07:00, 11:00] and [17:00, 22:00], reaching the daily peak, with a peak-trough difference of 772MW. Figure 7 reveals that, in contrast, Scheme 2 enables the furnace's participation in flexible system adjustments, ramping up power notably during [00:00, 07:00] and [12:00, 16:00] to accommodate more wind power. Consequently, the combined outputs of the four thermal units stabilize further compared to Scheme 1, reducing the day's peak-trough difference to 652MW.

Compared to Scheme 1, Scheme 2 taps into the flexibility potential of energy-intensive load furnaces. It elevates its consumption during wind-rich periods, enhancing the system's wind power absorption and reducing wind curtailment. Conversely, during wind-scarce periods, it curtails its consumption, alleviating system supply pressures, reducing dependency on thermal units, and thereby diminishing overall carbon emissions. To elucidate the 24-hour output fluctuations of each thermal unit under both schemes, we introduce the 'unit output fluctuation ratio' and plot the 24-hour clock charts for all four teams accordingly. The details follow:

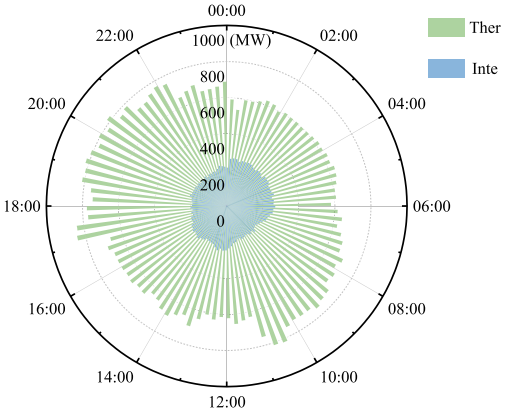

FIGURE 7. The output of thermal power units and the energy consumption of fused magnesium load (Scheme 2).

$$\Delta a = \frac{P_{\max\,av} - P_{\min\,av}}{P_{av}} \tag{33}$$

Within the Equation, $P_{\max\,av}$ represents the average output of the thermal power generation unit during peak periods, $P_{\min\,av}$ signifies the mean work during off-peak intervals, and P_{av} denotes the average production projected for the subsequent day.

Figures 8 and 9 illustrate the outputs from four thermal power units, designated as Unit 1 through Unit 4. A holistic view of both figures indicates a more steady output distribution across a 24-hour scheduling cycle for Scheme 2. In Figure 8, under Scheme 1, where high-capacity ferrosilicon loads are not considered for regulation, the four thermal units exhibit significant fluctuations, with an average 24-hour output of 665MW. During the intervals of [09:00, 12:00] and [17:00, 22:00], the output peaks, registering an overall average of 847MW, whereas the off-peak standard is 552MW. Consequently, the total fluctuation ratio, Δa, for Scheme 1 is approximately 0.4436. In contrast, Figure 9 depicts a Scheme where, upon incorporating detailed modeling of the high-capacity ferrosilicon load for regulation, each thermal unit's output is noticeably smoother compared to Scheme 1, with a 24-hour average work of 676MW. The peak and off-peak averages are 791MW and 623MW, respectively, resulting in a fluctuation ratio of 0.2485 for Scheme 2.

In summary, compared to Scheme 1, Scheme 2 demonstrates a pronounced reduction in output variability for the thermal units, resulting in reduced equipment wear and maintenance costs, decreased carbon emissions, streamlined

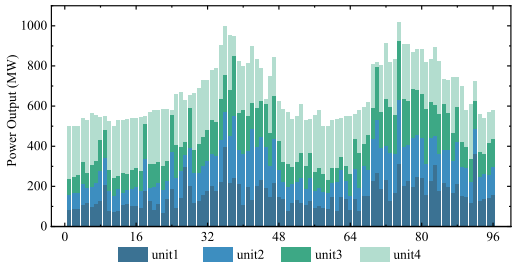

FIGURE 8. Output status of 4 thermal power units (Scheme 1).

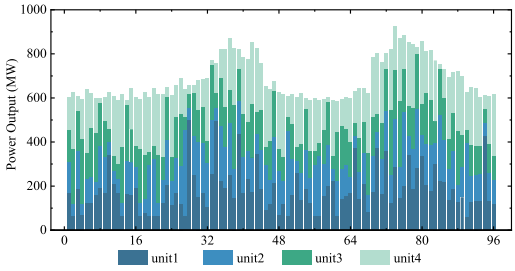

FIGURE 9. Output status of 4 thermal power units (Scheme 2).

power plant operational management, and improved thermal efficiency of the units.

On another note, to compare the wind power absorption capabilities of the electrical systems under different Schemes, Figures 10 and 11 illustrate the absorbed wind energy and curtailed wind energy for each respective strategy. In Figure 10, the parameters "W-pre," "W-1," and "W-2" represent the wind power output prediction, the wind power output under Scheme 1, and the wind power output under Scheme 2, respectively. Meanwhile, Figure 11 designate "Inte-curt" as the absorbed wind power quantity in Scheme 1 and "N-Inte-curt" as that in Scheme 2. An examination of Figure 11 reveals that under Scheme 1, the highest wind power curtailment periods are [23:00, 6:00] and [12:00, 16:30]. Collectively, these intervals account for approximately 90% of the total curtailed wind power over the scheduling cycle, with a peak curtailment of up to 98 MWh within a single period. In contrast, with the incorporation of high-capacity ferrosilicon load regulation in Scheme 2, the maximum curtailment in a single interval is reduced to 37 MWh, signifying a notable overall reduction in wind power curtailment.

Tables 2 and 3 elucidate the curtailment penalty costs, the unit operational costs of the thermal power units, and the total costs under both Schemes, while Figure 12 provides a comparative illustration of the team operational costs of the thermal power units.

Tables 2 and 3 show that the operational costs of the thermal power units in both Schemes are comparable. However, compared to Scheme 1, the curtailment penalty costs in Scheme 2 are significantly reduced, consequently leading to an overall cost reduction in system operations for Scheme 2. The variance in operational strategies has a negligible impact

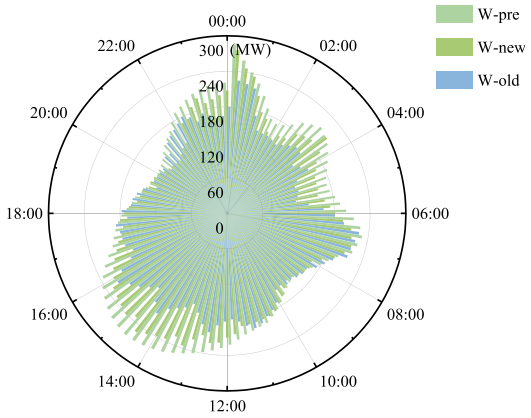

FIGURE 10. Comparison of wind power consumption under different schemes.

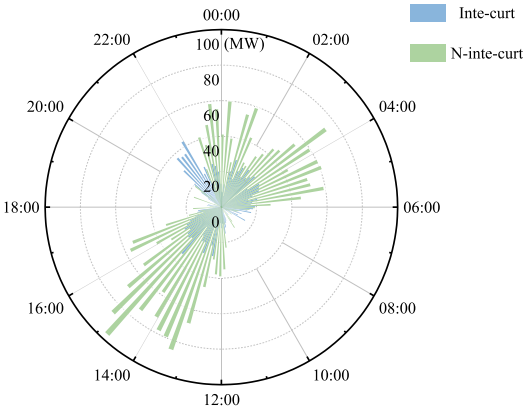

FIGURE 11. Comparison of wind curtailment under different schemes.

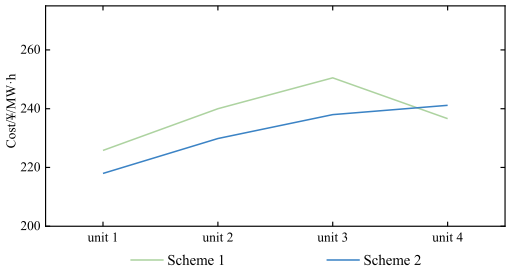

FIGURE 12. Comparison of unit operating costs of thermal power units under different schemes.

TABLE 2. Comparison of system operating cost under different schemes.

Scheme	M_W/¥	M_G/¥	C_{total}
Scheme 1	254039	379458	633497
Scheme 2	129637	383641	513278

on the per-unit operating cost of the thermal power units. A comparative representation of the total operational costs for both Schemes across different time slots is depicted in Figure 13.

TABLE 3. Comparison of unit operating costs of thermal power units under different schemes.

Thermal power unit	Scheme 1/ (¥/MW·h)	Scheme 2/ (¥/MW·h)	Cost spread /(¥/MW·h)
1	225.8082	217.9621	-7.8471
2	231.5661	229.8590	-1.7071
3	250.4062	247.2230	-3.1832
4	236.6025	241.1665	4.5640

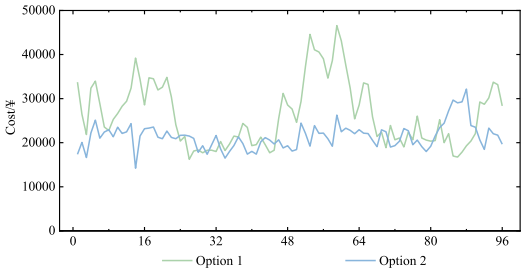

FIGURE 13. Comparison chart of total system operating costs under different schemes.

Figure 13 clearly illustrates that during the time intervals [23:00, 06:00] and [12:00, 16:30], the total operational cost under Scheme 2 experiences a substantial decrease, registering a reduction of 25.35% compared to Scheme 1. This observation aligns with the curtailment patterns shown in Figure 11, reinforcing the conclusion that wind power absorption is notably enhanced in these intervals under Scheme 2. Over the entire scheduling period, the system operational cost under Scheme 2 is reduced by 18.97% relative to Scheme 1.

V. CONCLUSION

This study introduced an optimization scheduling method to enhance wind power integration capabilities and minimize system operational costs in the power grid, incorporating a detailed modeling approach for energy-intensive electric arc furnace loads. The proposed methodology utilizes a two-tier structure. The upper layer analyzes the operational characteristics of the energy-intensive electric arc furnace to optimize wind power consumption. This approach utilizes the electric arc furnace's load regulation ranges, employing its detailed model to guarantee effective wind power absorption enhancement. Based on this upper model, the subsequent layer integrates the operational costs of thermal power units and the penalty costs associated with wind power curtailment, constructing an optimization model to minimize overall system costs. Through illustrative case studies, the method demonstrated its superior performance in addressing challenges such as wind power consumption and system operational cost management, in contrast to conventional optimization strategies that overlook the load regulation potential of energy-intensive electric arc furnaces.

However, despite the significant strides made in this research, certain limitations remain. During the modeling phase for electric arc furnace control, the study failed to meticulously consider the production scheduling tasks of electric arc furnace enterprises, nor did it adequately account for the production capabilities and regulation response engagement of these enterprises under varying industrial prosperity levels. These oversight areas hint at the directions for future research endeavors.

CONFLICT OF INTEREST DISCLOSURE

The authors of this manuscript hereby confirm that there are no potential conflicts of interest related to the content and outcomes of this research.

REFERENCES

[1] Int. Energy Agency. *Wind*. Accessed: May 18, 2021. [Online]. Available: https://www.iea.org/energy-system/renewables/wind

[2] J. Dong, F. Gao, X. Guan, Q. Zhai, and J. Wu, "Storage sizing with peak-shaving policy for wind farm based on cyclic Markov chain model," *IEEE Trans. Sustain. Energy*, vol. 8, no. 3, pp. 978–989, Jul. 2017, doi: 10.1109/TSTE.2016.2637916.

[3] N. Ding, J. Duan, S. Xue, M. Zeng, and J. Shen, "Overall review of peaking power in China: Status quo, barriers and solutions," *Renew. Sustain. Energy Rev.*, vol. 42, pp. 503–516, Feb. 2015, doi: 10.1016/j.rser.2014.10.041.

[4] R. Ma, K. Li, X. Li, and Z. Qin, "Economic and low-carbon day-ahead Pareto-optimal scheduling for wind farm integrated power systems with demand response," *J. Mod. Power Syst. Clean Energy*, vol. 3, no. 3, pp. 393–401, Sep. 2015, doi: 10.1007/s40565-014-0094-7.

[5] H. Ma, H. Wang, Z. Yan, and Q. Yu, "Evaluating peak-regulation capability for power grid with various energy resources in Chinese urban regions via a pragmatic visualization method," *Sustain. Cities Soc.*, vol. 80, May 2022, Art. no. 103749, doi: 10.1016/j.scs.2022.103749.

[6] A. Alzahrani, G. Hafeez, G. Rukh, S. Murawwat, F. Iftikhar, S. Ali, S. I. Haider, M. I. Khan, and A. M. Abed, "Demand response for optimal power usage scheduling considering time and power flexibility of load in smart grid," *IEEE Access*, vol. 11, pp. 33640–33651, 2023, doi: 10.1109/ACCESS.2023.3263849.

[7] Z. Liu, Z. Xiao, Y. Wu, H. Hou, T. Xu, Q. Zhang, and C. Xie, "Integrated optimal dispatching strategy considering power generation and consumption interaction," *IEEE Access*, vol. 9, pp. 1338–1349, 2021, doi: 10.1109/ACCESS.2020.3045151.

[8] J. Domínguez-Jiménez, N. Henao, K. Agbossou, A. Parrado, J. Campillo, and S. H. Nagarsheth, "A stochastic approach to integrating electrical thermal storage in distributed demand response for Nordic communities with wind power generation," *IEEE Open J. Ind. Appl.*, vol. 4, pp. 121–138, 2023, doi: 10.1109/OJIA.2023.3264651.

[9] A. Yousefi, H. H. Iu, T. Fernando, and H. Trinh, "An approach for wind power integration using demand side resources," *IEEE Trans. Sustain. Energy*, vol. 4, no. 4, pp. 917–924, Oct. 2013, doi: 10.1109/TSTE.2013.2256474.

[10] G. Cai, J. Zhou, Y. Wang, H. Zhang, A. Sun, and C. Liu, "Multi-objective coordinative scheduling of system with wind power considering the regulating characteristics of energy-intensive load," *Int. J. Electr. Power Energy Syst.*, vol. 151, Sep. 2023, Art. no. 109143, doi: 10.1016/j.ijepes.2023.109143.

[11] K. Tang, S. Fang, G. Chen, and T. Niu, "Unit maintenance strategy considering the uncertainty of energy intensive load and wind power under the carbon peak and carbon neutral target," *IEEE Access*, vol. 11, pp. 38819–38827, 2023, doi: 10.1109/ACCESS.2023.3267274.

[12] B. A. Franco, P. Baptista, R. C. Neto, and S. Ganilha, "Assessment of offloading pathways for wind-powered offshore hydrogen production: Energy and economic analysis," *Appl. Energy*, vol. 286, Mar. 2021, Art. no. 116553, doi: 10.1016/j.apenergy.2021.116553.

[13] S. Liao, J. Xu, Y. Sun, and Y. Bao, "Local utilization of wind electricity in isolated power systems by employing coordinated control scheme of industrial energy-intensive load," *Appl. Energy*, vol. 217, pp. 14–24, May 2018, doi: 10.1016/j.apenergy.2018.02.103.

[14] Y. Zhang, W. Ningbo, K. Ding, Q. Zhou, P. Gao, and Z. Zhang, "The key technology of the coordinated control system of wind power and energy-intensive load," in *Proc. 4th Int. Conf. Intell. Green Building Smart Grid (IGBSG)*, Hubei, China, Sep. 2019, pp. 349–353, doi: 10.1109/IGBSG.2019.8886294.
[15] H. Yang, Q. Yu, J. Liu, Y. Jia, G. Yang, E. Ackom, and Z. Y. Dong, "Optimal wind-solar capacity allocation with coordination of dynamic regulation of hydropower and energy intensive controllable load," *IEEE Access*, vol. 8, pp. 110129–110139, 2020, doi: 10.1109/ACCESS.2020.3001666.
[16] X. Li, X. Cao, C. Li, B. Yang, M. Cong, and D. Chen, "A coordinated peak shaving strategy using neural network for discretely adjustable energy-intensive load and battery energy storage," *IEEE Access*, vol. 8, pp. 5331–5338, 2020, doi: 10.1109/ACCESS.2019.2962814.
[17] K. Liu and F. Gao, "Scenario adjustable scheduling model with robust constraints for energy intensive corporate microgrid with wind power," *Renew. Energy*, vol. 113, pp. 1–10, Dec. 2017, doi: 10.1016/j.renene.2017.05.056.
[18] State Council, People's Republic China. *Haicheng Investment Guide*. Accessed: Oct. 28, 2021. [Online]. Available: https://files.anshan.gov.cn
[19] State Grid Liaoning Electric Power Supply Co. Ltd. *Qingjie Dianneng Shouhu Liaoning Bihai Lantian*. Accessed: Jun. 3, 2021. [Online]. Available: https://www.in.sgcc.com.cn
[20] W. Wang, T. Chai, H. Wang, and Z. Wu, "Signal-compensation-based adaptive PID control for fused magnesia smelting processes," *IEEE Trans. Ind. Electron.*, vol. 70, no. 9, pp. 9441–9451, Sep. 2023.
[21] Z. Wu, Y. Wu, T. Chai, and J. Sun, "Data-driven abnormal condition identification and self-healing control system for fused magnesium furnace," *IEEE Trans. Ind. Electron.*, vol. 62, no. 3, pp. 1703–1715, Mar. 2015, doi: 10.1109/TIE.2014.2349479.
[22] Z. Wu, T. Liu, Z.-P. Jiang, T. Chai, and L. Zhang, "Nonlinear control tools for fused magnesium furnaces: Design and implementation," *IEEE Trans. Ind. Electron.*, vol. 65, no. 9, pp. 7248–7257, Sep. 2018, doi: 10.1109/TIE.2017.2767545.
[23] L. Ning, A. Sun, K. Liang, H. He, Z. Jiao, C. Liu, Y. Wang, and H. Zhang, "Research on day-ahead peak load regulation strategy of fused magnesium load based on genetic algorithm," in *Proc. IEEE Int. Conf. Electr. Eng. Mechatronics Technol. (ICEEMT)*, Qingdao, China, Jul. 2021, pp. 714–719, doi: 10.1109/ICEEMT52412.2021.9601737.

YIBO WANG (Member, IEEE) was born in Shandong, China, in 1989. He received the B.S., M.S., and Ph.D. degrees in electrical engineering from Northeast Electric Power University, Jilin, China, in 2010, 2016, and 2020, respectively. Since 2020, he has been a Teacher with the School of Electrical Engineering, Northeast Electric Power University. His current research interests include renewable energy integration into power networks, power systems, and power quality.

ZIKANG YANG was born in Hebei, China, in 1999. He received the B.S. degree in civil engineering from Northeast Electric Power University, Jilin, China, in 2021, where he is currently pursuing the master's degree in electrical engineering. His current research interests include hybrid transformers and power quality.

XUDONG ZHAO was born in Heilongjiang, China, in 1999. He received the Bachelor of Engineering degree in electrical engineering from Northeast Electric Power University, in 2021, where he is currently pursuing the master's degree in electrical engineering. His primary research focus is on the demand-side response of power systems.

HONGDAN LIU was born in Shandong, China, in 1998. She received the B.S. degree from Shijiazhuang Tiedao University Sifang College, in 2022. She is currently pursuing the master's degree in electrical engineering with Northeast Electric Power University. Her research interests include renewable energy integration into power networks and power systems.

DONGZHE WANG was born in Hebei, China, in 1999. He received the B.S. degree in electrical engineering from the Science and Technology College, North China Electric Power University, Hebei, in 2021. He is currently pursuing the master's degree in electrical engineering with Northeast Electric Power University. His current research interest includes power system dispatch.

CHUANG LIU (Member, IEEE) received the M.S. degree from Northeast Electric Power University, Jilin, China, in 2009, and the Ph.D. degree from Harbin Institute of Technology, Harbin, China, in 2013, both in electrical engineering. From 2010 to 2012, he was with the Future Energy Electronics Center, Virginia Polytechnic Institute and State University, Blacksburg, VA, USA, as a Visiting Ph.D. Student, supported by the Chinese Scholarship Council. In 2013, he became an Associate Professor with the School of Electrical Engineering, Northeast Electric Power University, where he has been a Professor, since 2016. His research interests include power-electronics-based on ac and dc transformers for future hybrid ac–dc power grids, flexible operation and control of power grid based on ac–ac transformation, and power electronics-based power system stability analysis and control.